# One-step Preparation of Amorphous Citrate-Chelated CoNiFe Trimetallic Hydroxides for Oxygen Evolution Reaction

Jiaqi Zhou,[a] Yuhong Zhang,[a] Tianrui Yu,[a] Tong Wang,[a] Chuangyi Tong,[a] Mingxin Feng,[a] Zewu Zhang,[b] Jiehua Bao*[b] and Yuming Zhou*[a]

[a] School of Chemistry and Chemical Engineering, Southeast University, Jiangsu Optoelectronic Functional Materials and Engineering Research Center, Nanjing, 211100, Jiangsu Province, China

[b] School of Materials Science and Engineering, Nanjing Institute of Technology, Nanjing, 211167, Jiangsu Province, China

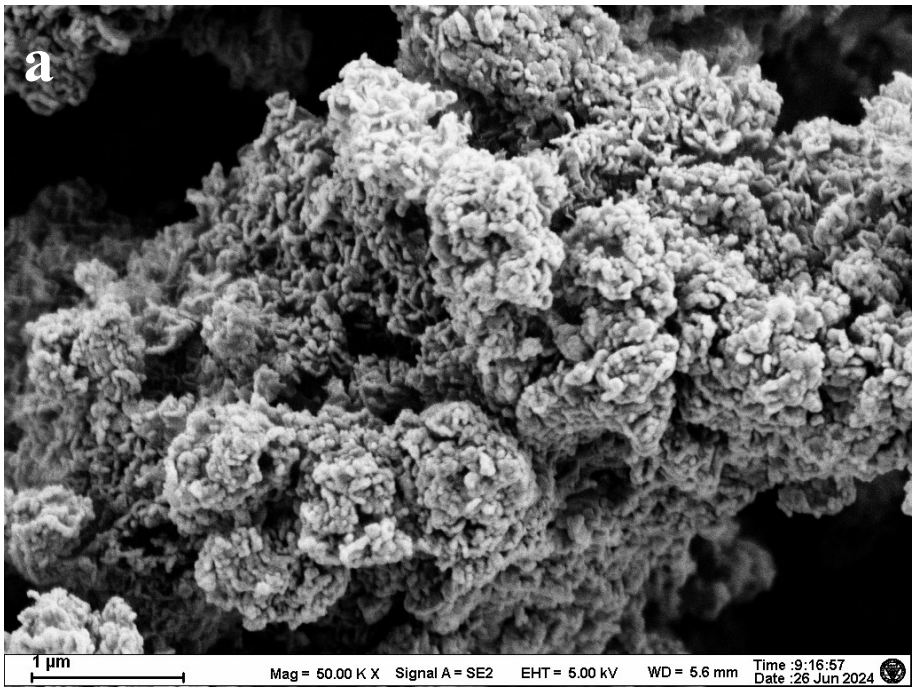


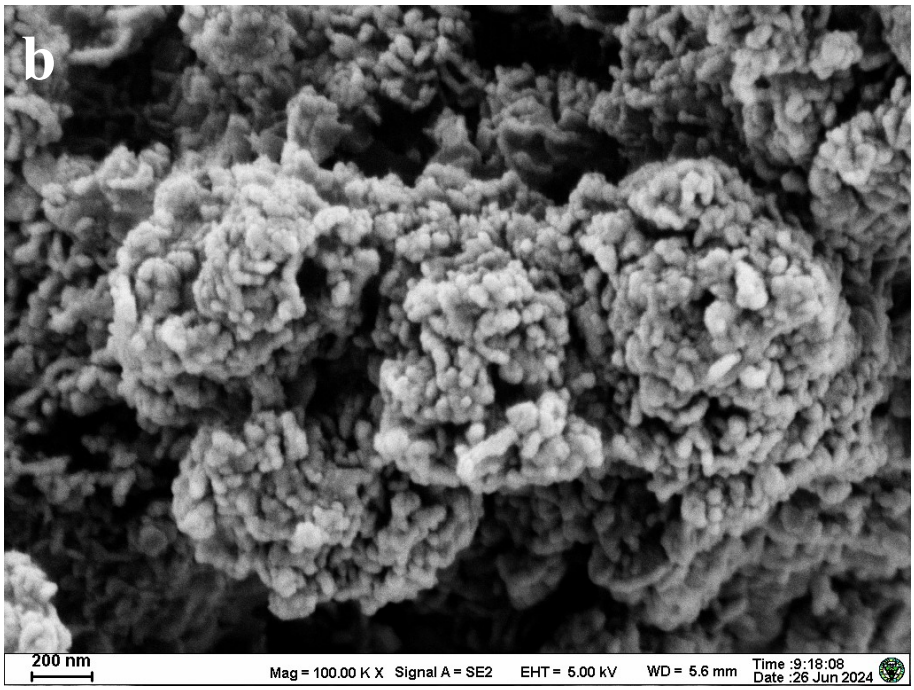


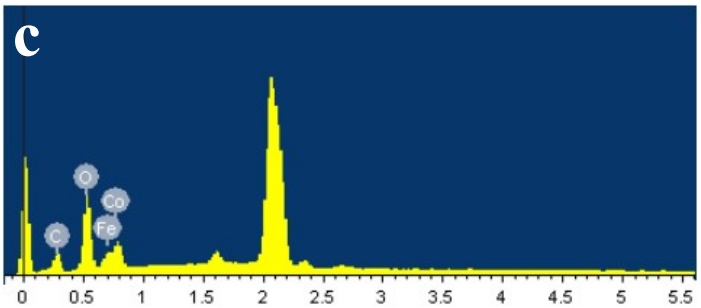


| | At% |
|---|---|
| C K | 34.36 |
| O K | 43.12 |
| Fe K | 6.24 |
| Co K | 16.28 |

Figure S1. (a-b) SEM images and (c) EDX result of $Co_3Fe$-W.

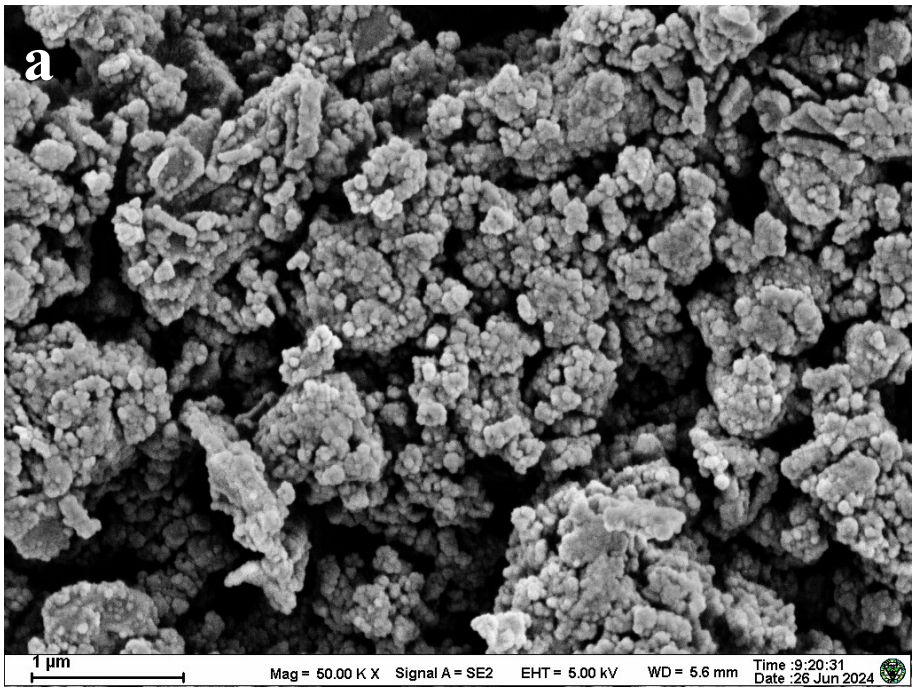


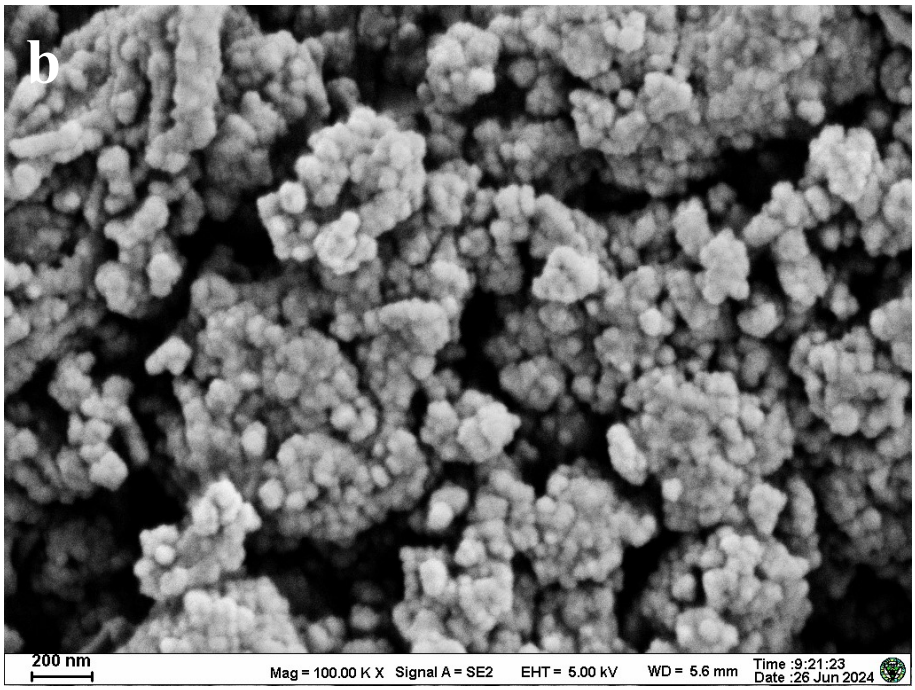


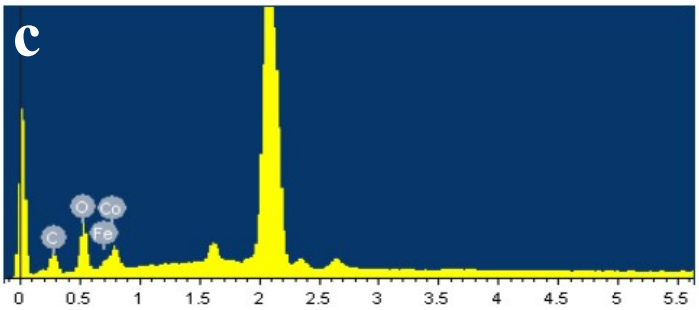


| | At% |
|---|---|
| C K | 31.64 |
| O K | 42.19 |
| Fe K | 5.99 |
| Co K | 20.18 |

Figure S2. (a-b) SEM images and (c) EDX result of $Co_3Fe$-E.

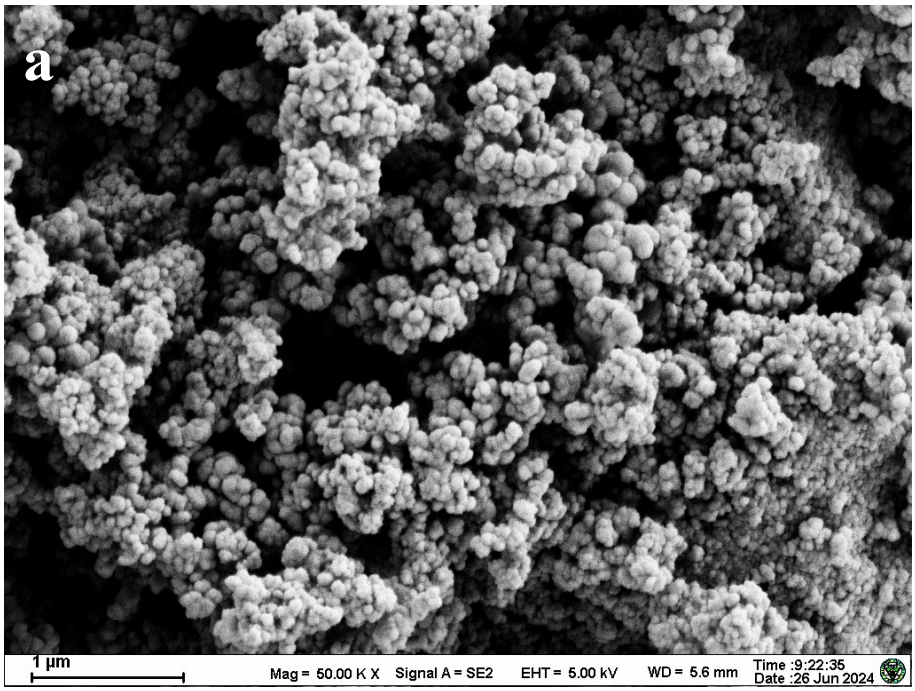


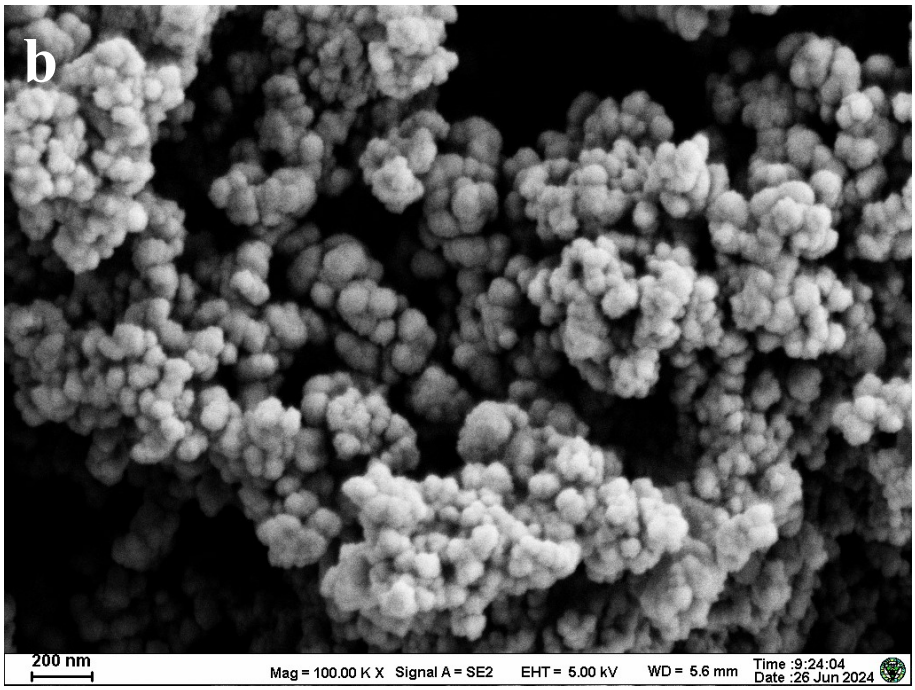


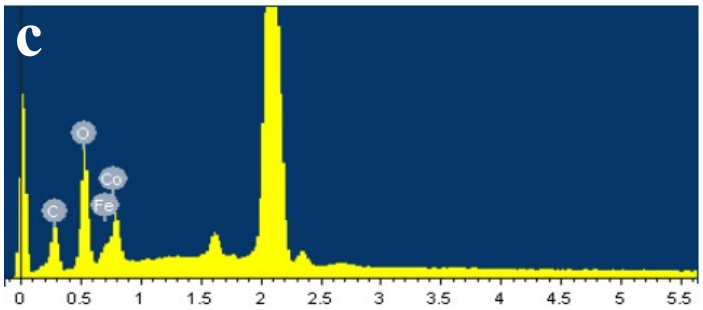


| | At% |
|---|---|
| C K | 32.31 |
| O K | 44.48 |
| Fe K | 5.27 |
| Co K | 17.94 |

Figure S3. (a-b) SEM images and (c) EDX result of $Co_3Fe$-W/E.

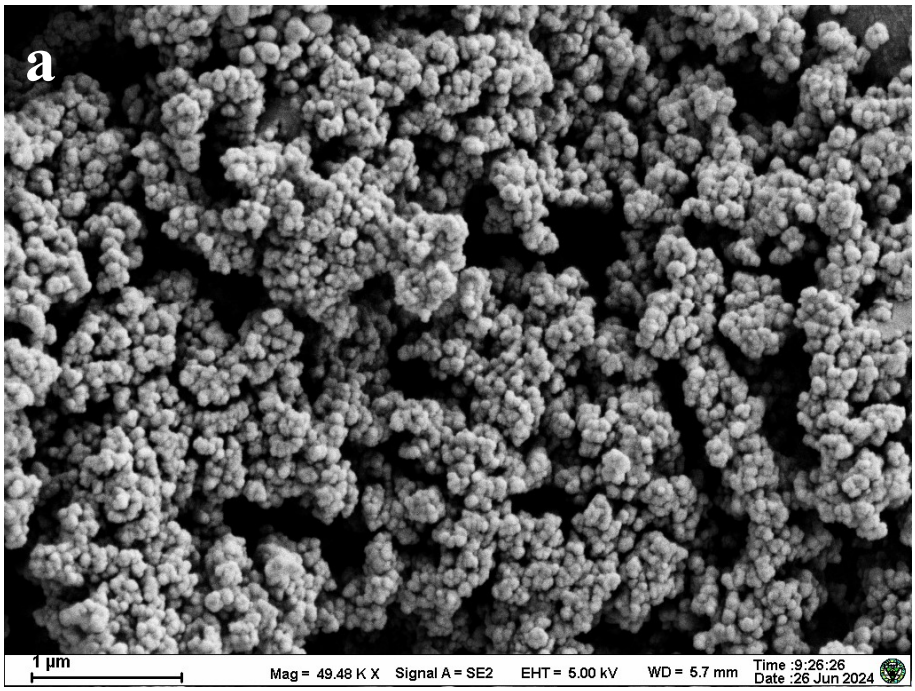


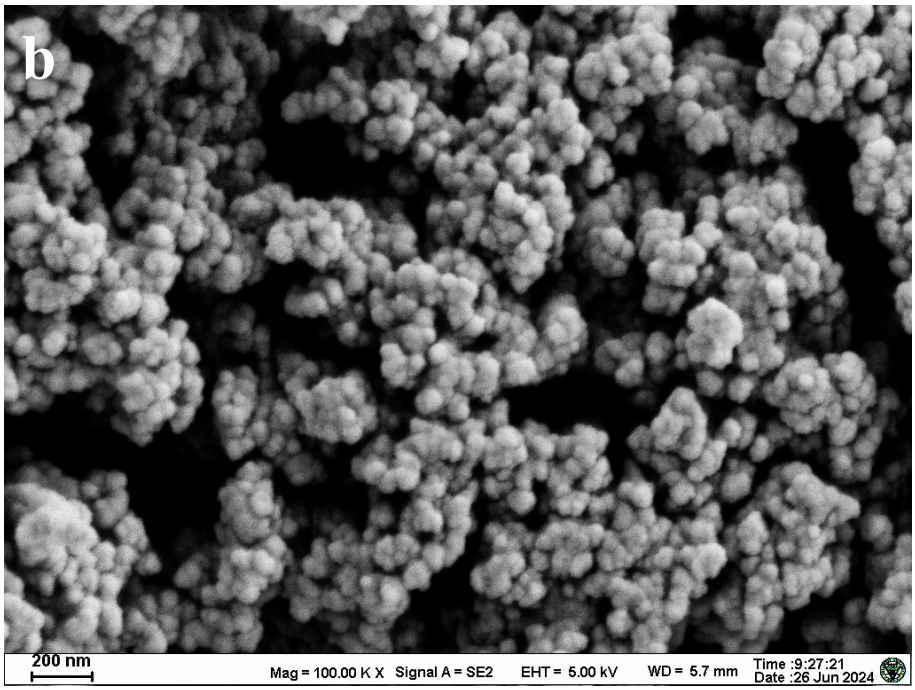


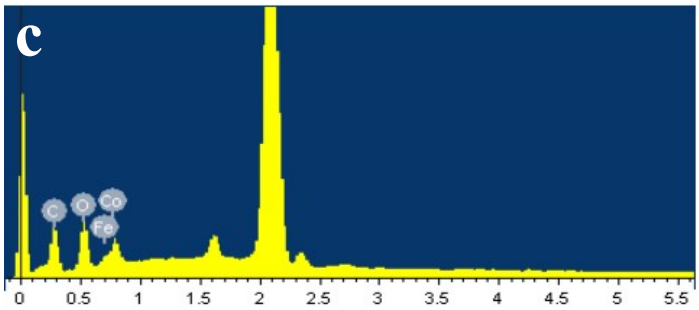


| | At% |
|---|---|
| C K | 55.89 |
| O K | 30.67 |
| Fe K | 3.19 |
| Co K | 9.25 |

Figure S4. (a-b) SEM images and (c) EDX result of $Co_3Fe$-CA.

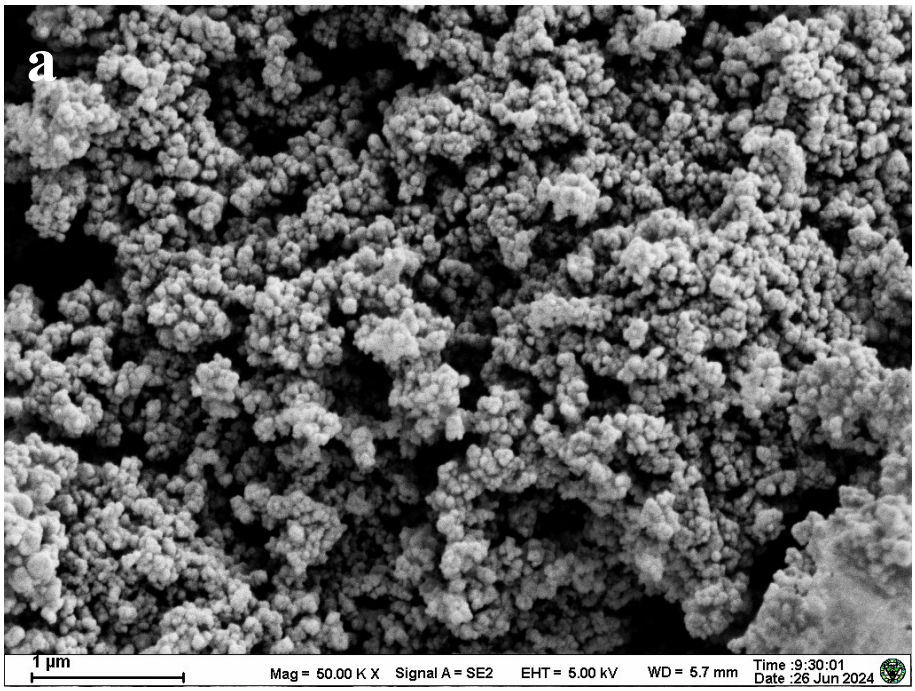


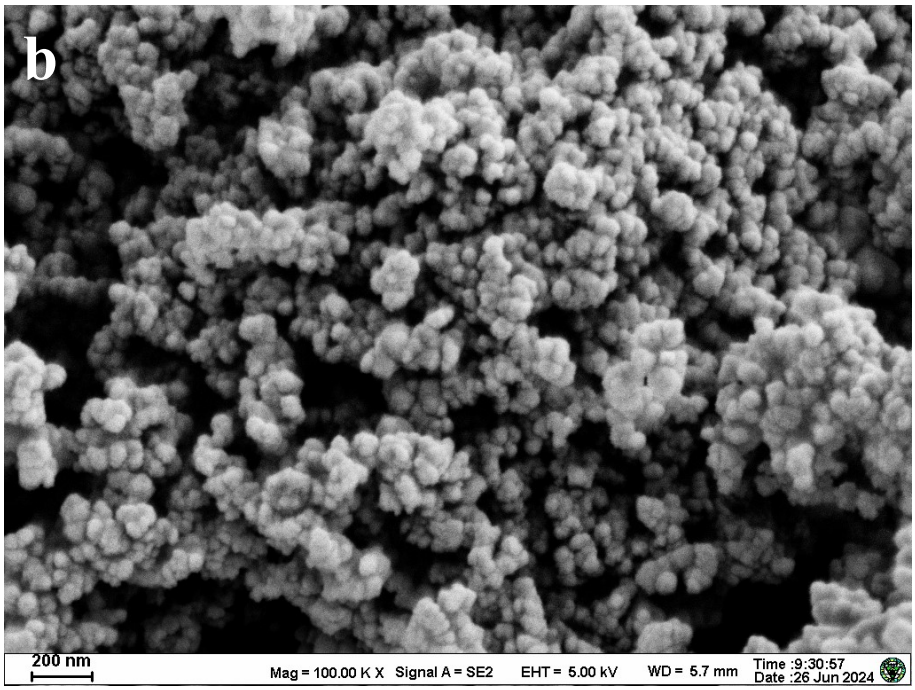


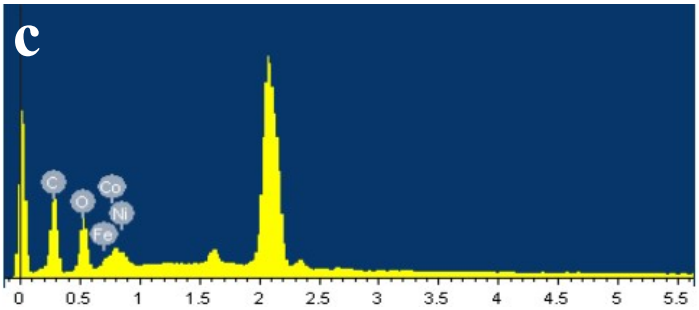


| | At% |
|---|---|
| C K | 60.27 |
| O K | 29.28 |
| Fe K | 2.49 |
| Co K | 5.18 |
| Ni K | 2.78 |

Figure S5. (a-b) SEM images and (c) EDX result of $Co_2NiFe$-CA.

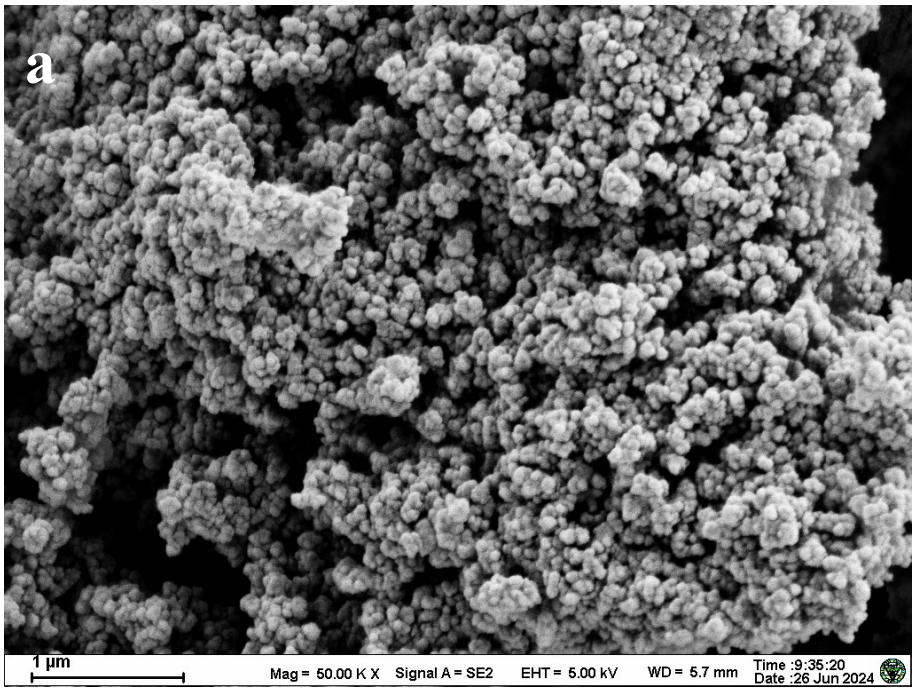


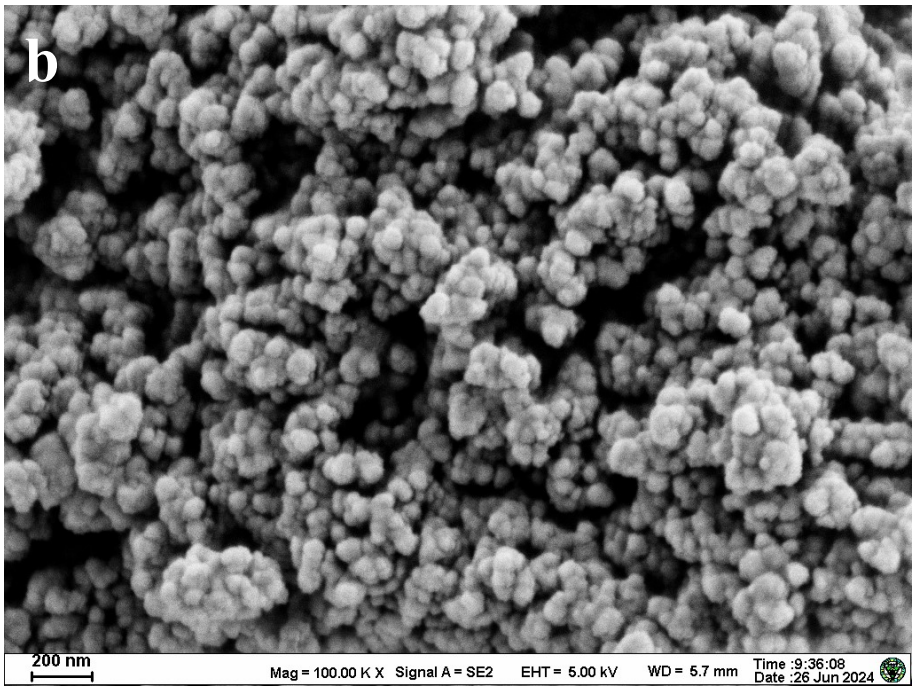


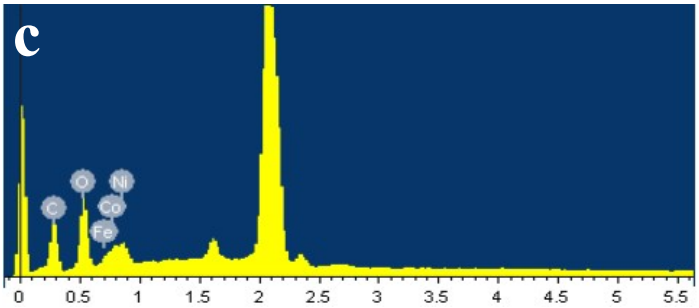


| | At% |
|---|---|
| C K | 54.32 |
| O K | 32.42 |
| Fe K | 3.44 |
| Co K | 5.27 |
| Ni K | 4.55 |

Figure S6. (a-b) SEM images and (c) EDX result of $Co_{1.5}Ni_{1.5}Fe$-CA.

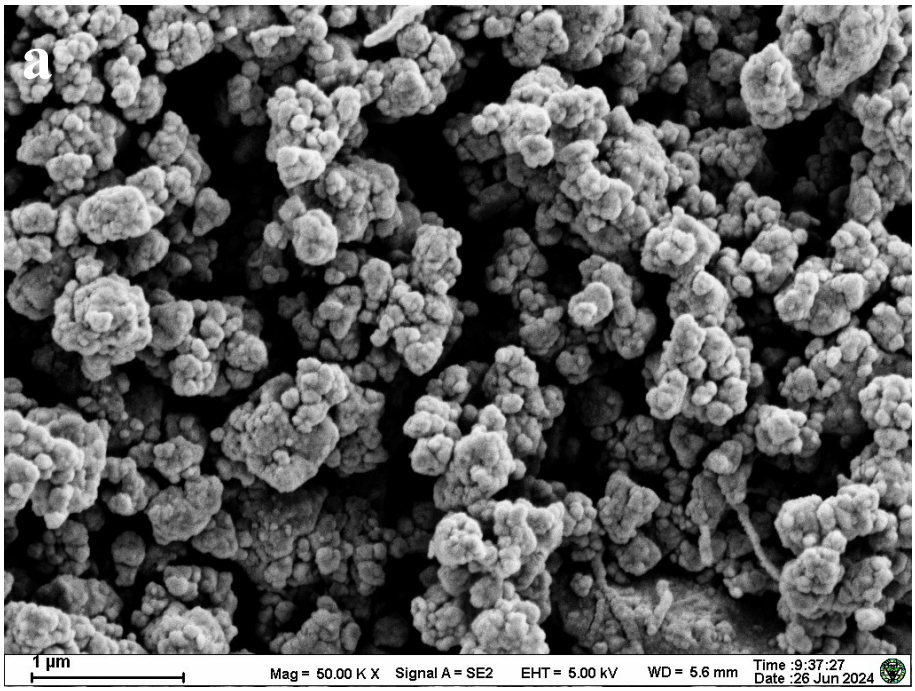


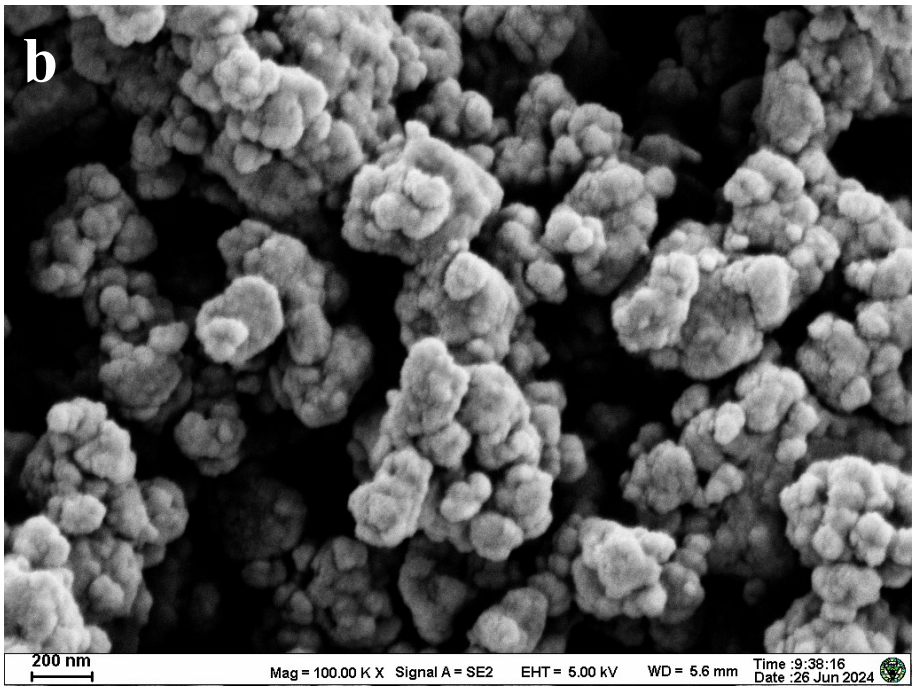


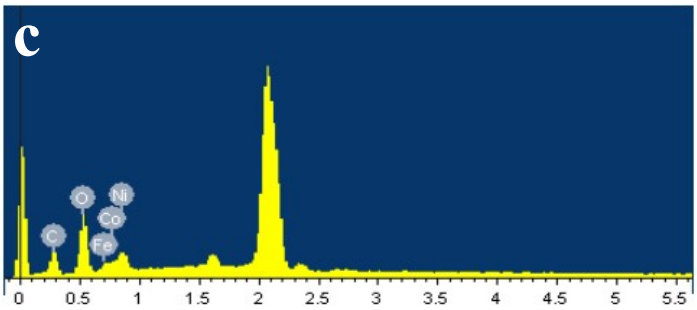


| | At% |
|---|---|
| C K | 52.25 |
| O K | 32.81 |
| Fe K | 3.61 |
| Co K | 4.06 |
| Ni K | 7.27 |

Figure S7. (a-b) SEM images and (c) EDX result of $CoNi_2Fe$-CA.

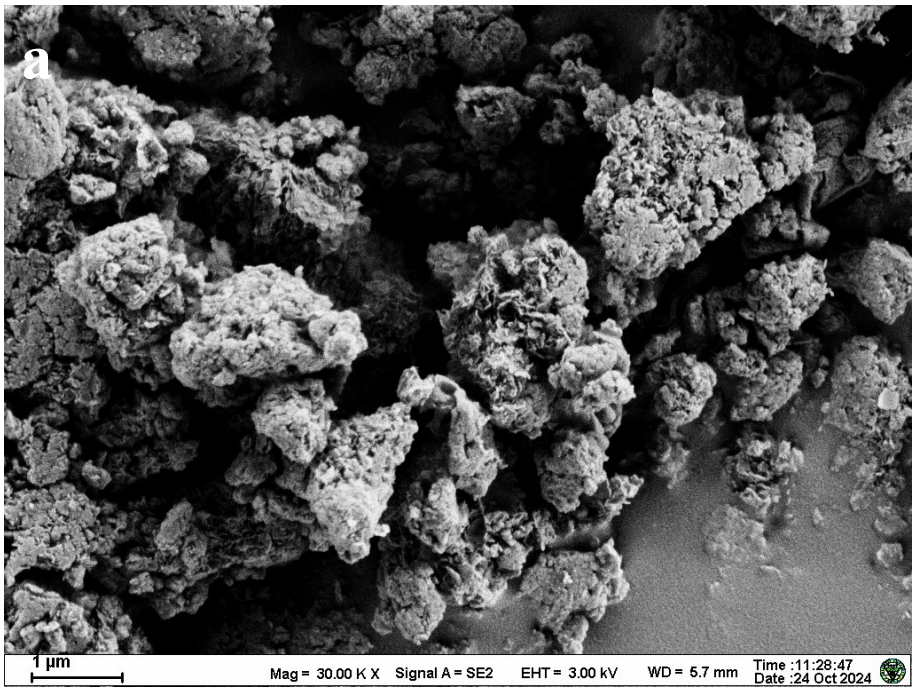


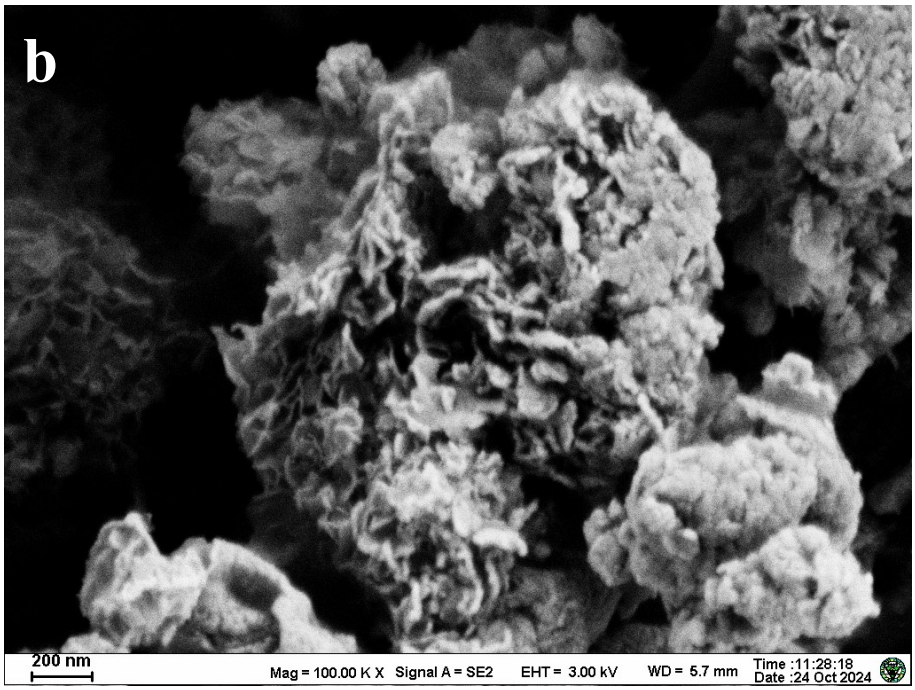


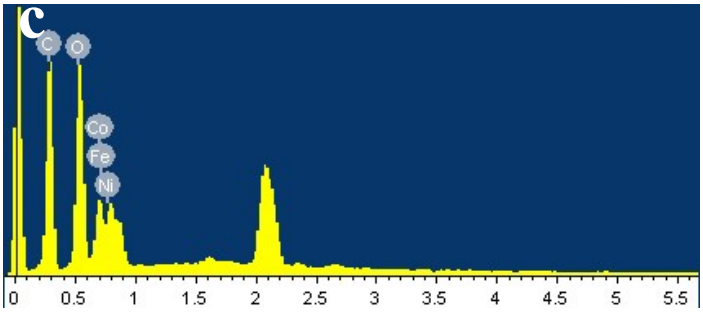


| | At% |
|---|---|
| C K | 55.96 |
| O K | 38.34 |
| Fe K | 1.44 |
| Co K | 2.73 |
| Ni K | 1.53 |

Figure S8. (a-b) SEM images and (c) EDX result of $Co_2NiFe$-CS.

Figure S9. (a-f) Size distribution of the (a) $Co_3Fe$-E, (b) $Co_3Fe$-W/E, (c) $Co_3Fe$-CA, (d) $Co_2NiFe$-CA, (e) $Co_{1.5}Ni_{1.5}Fe$-CA and (f) $CoNi_2Fe$-CA.

a

b

c

d

e

f

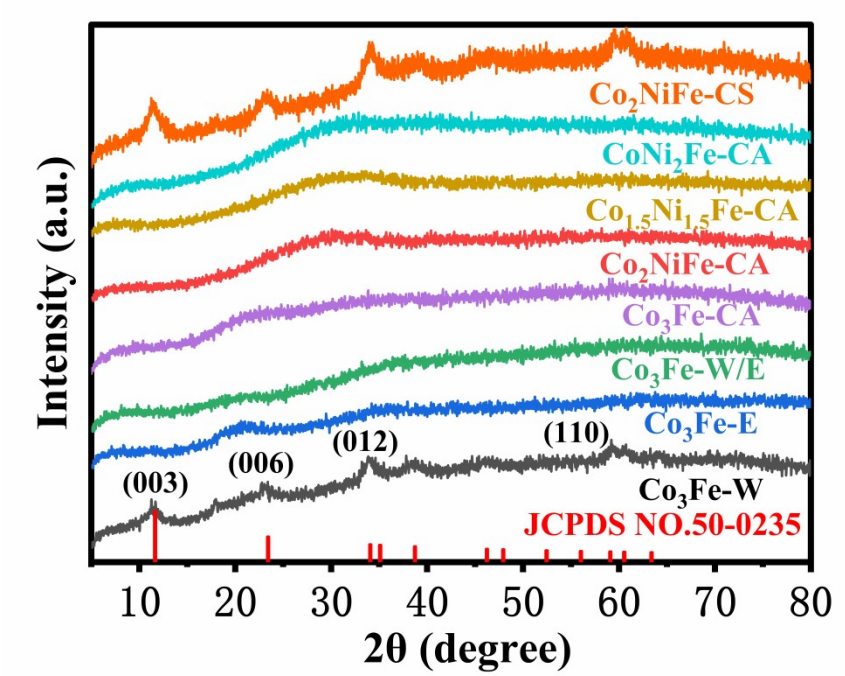


Figure S10. XRD images of all catalysts.

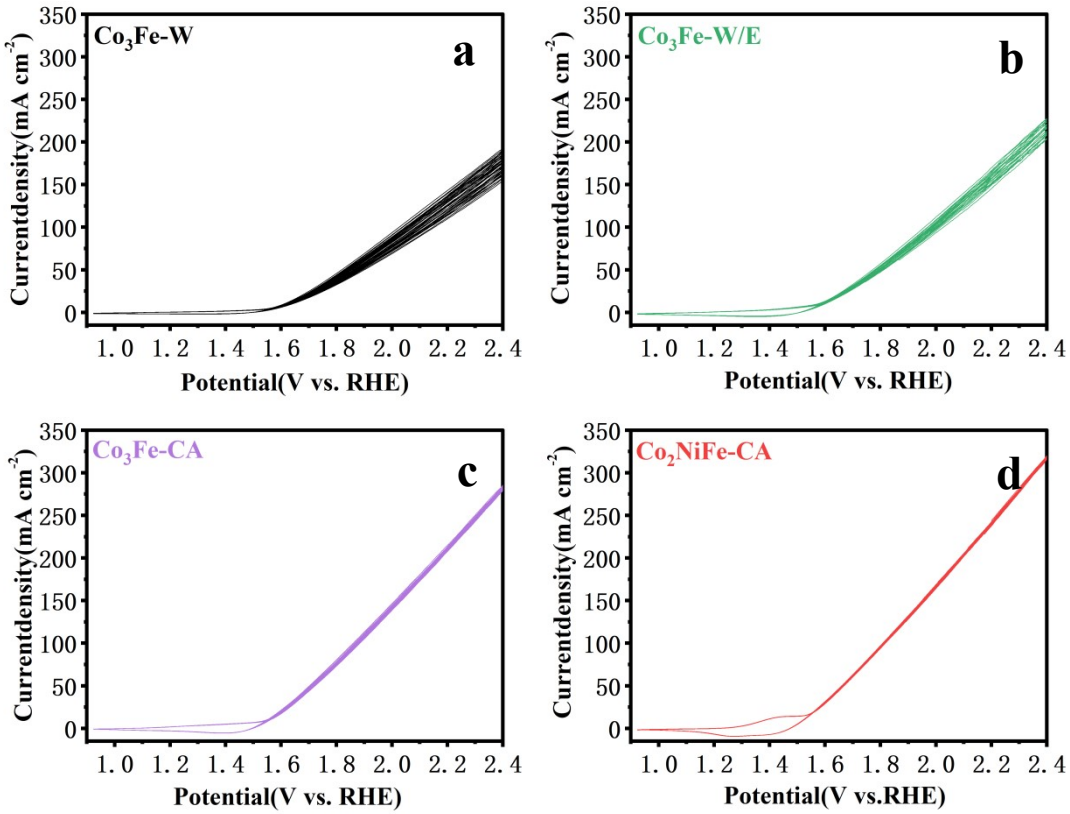


Figure S11. (a-d) CV curves of the (a) $Co_3Fe$-W, (b) $Co_3Fe$-W/E, (c) $Co_3Fe$-CA and (d) $Co_2NiFe$-CA.

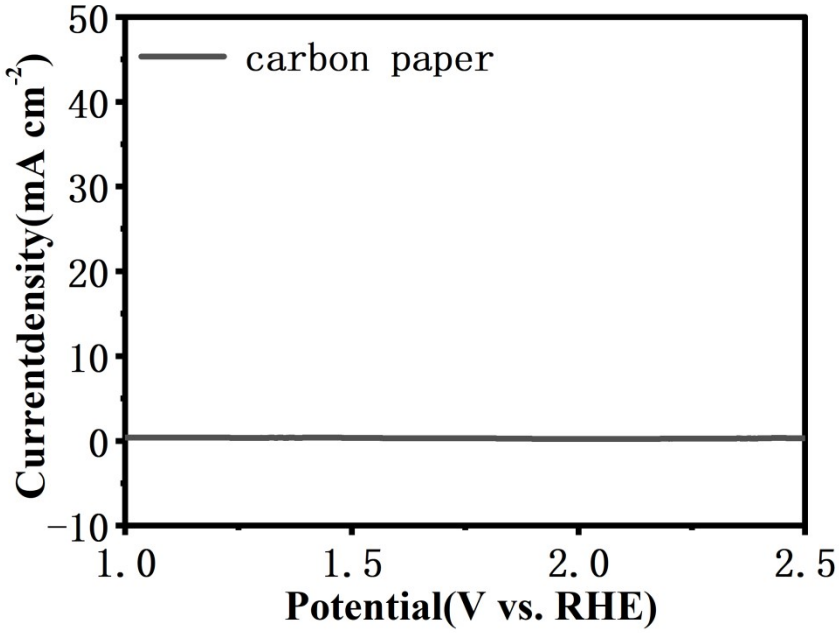


Figure S12. OER activity of carbon paper.

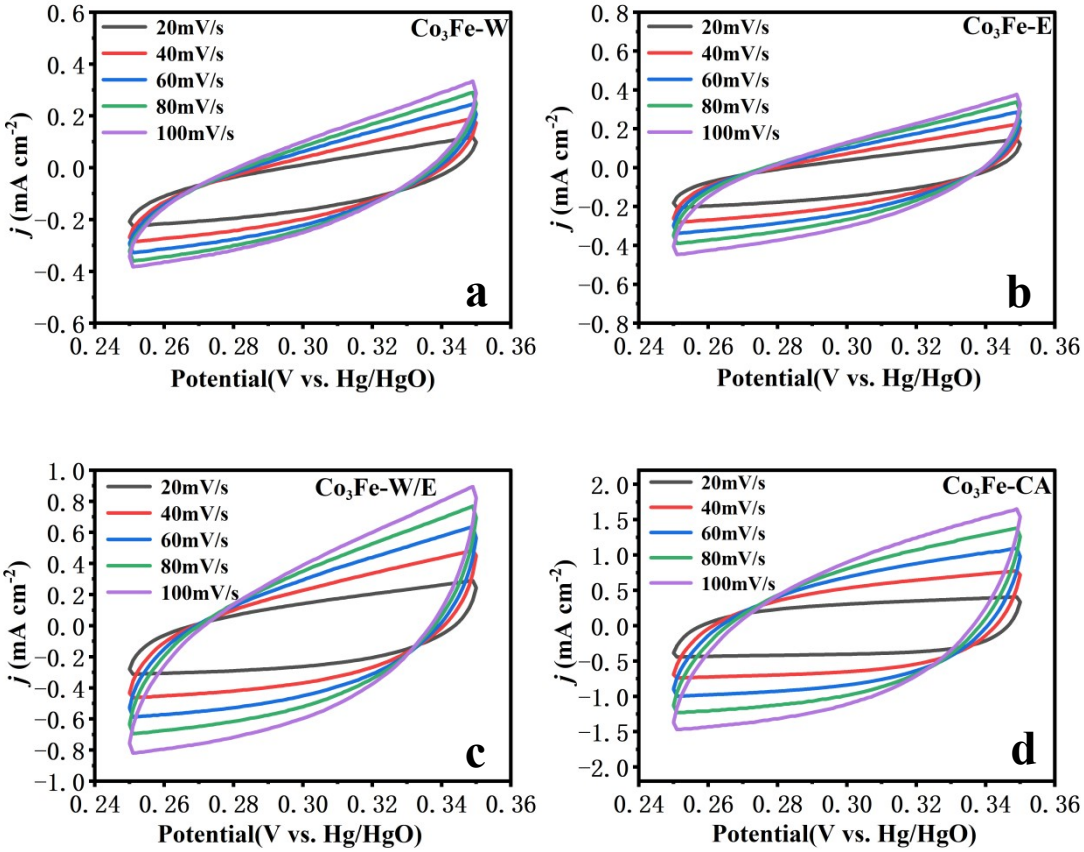

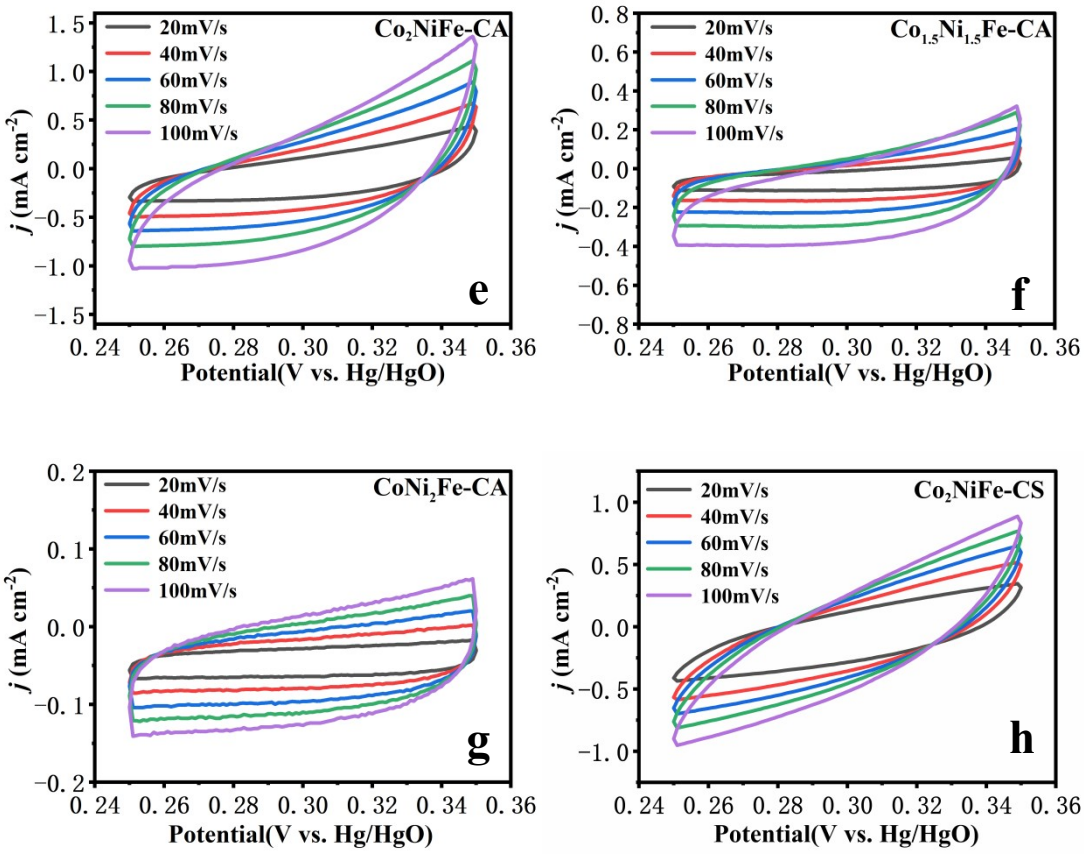


Figure S13. (a-h) CV curves of the (a) $Co_3Fe$-W, (b) $Co_3Fe$-E, (c) $Co_3Fe$-W/E, (d) $Co_3Fe$-CA, (e) $Co_2NiFe$-CA, (f) $Co_{1.5}Ni_{1.5}Fe$-CA, (g) $CoNi_2Fe$-CA and (h) $Co_2NiFe$-CS.

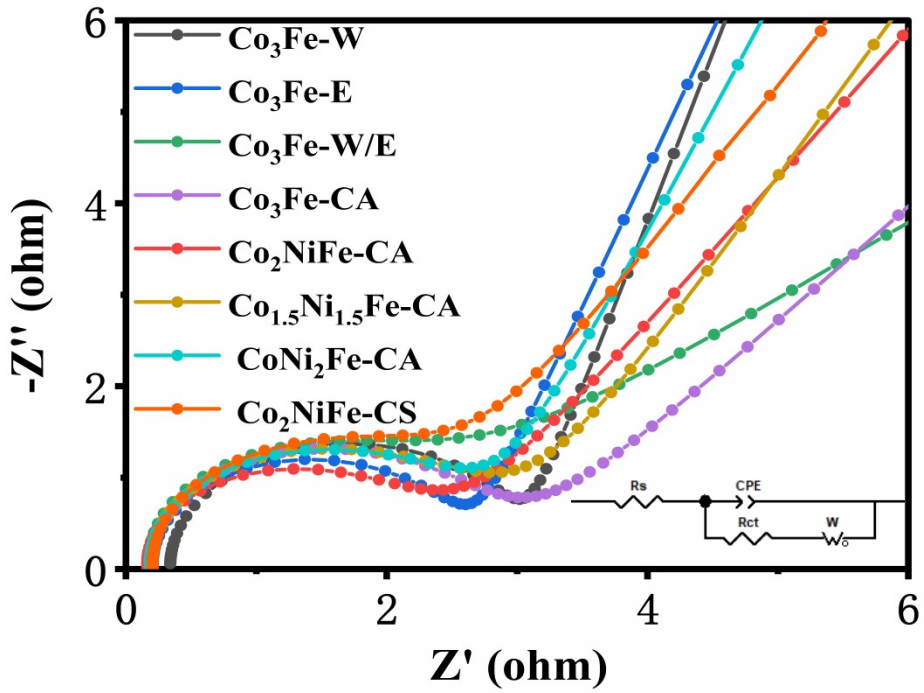


Figure S14. Nyquist plots for all catalysts.

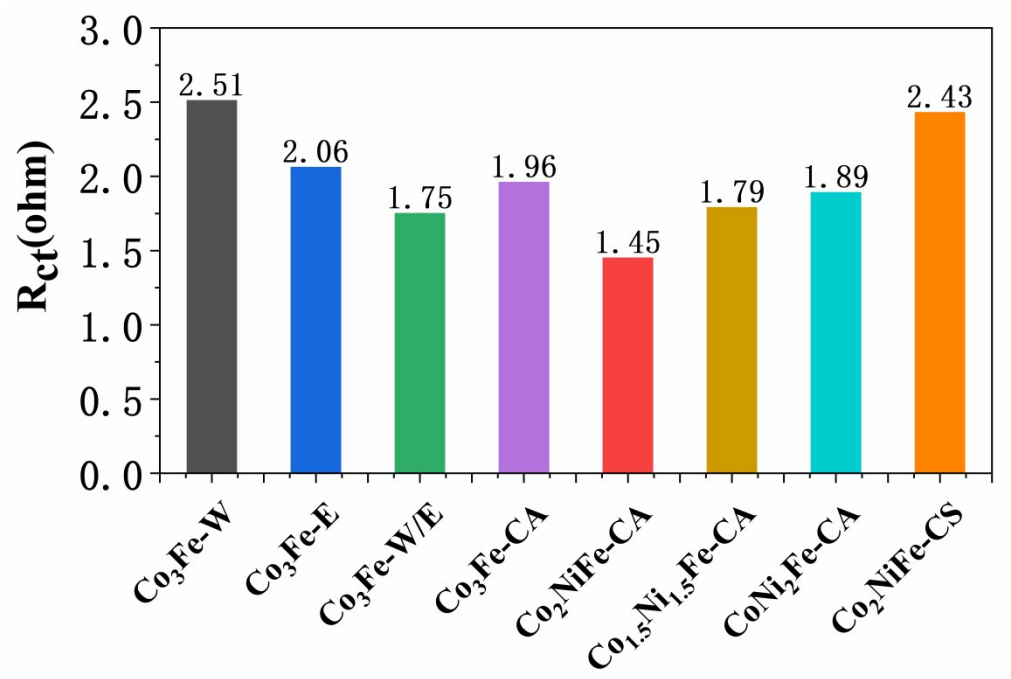


Figure S15. The values of $R_{ct}$.

**a** **b**

**c** **d**

e f

g h

Figure S16. (a-h) Chronopotentiometric curves of the (a) $Co_3Fe$-W, (b) $Co_3Fe$-E, (c) $Co_3Fe$-W/E, (d) $Co_3Fe$-CA, (e) $Co_2NiFe$-CA, (f) $Co_{1.5}Ni_{1.5}Fe$-CA, (g) $CoNi_2Fe$-CA and (h) $Co_2NiFe$-CS at 10 mA $cm^{-2}$.

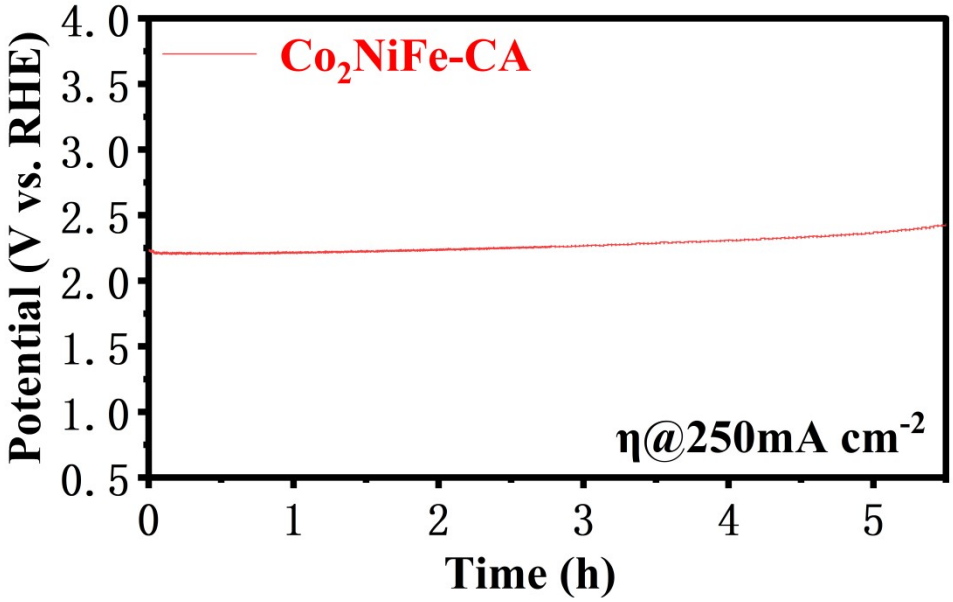


Figure S17. Chronopotentiometric curve of the $Co_2NiFe$-CA at 250 mA $cm^{-2}$.

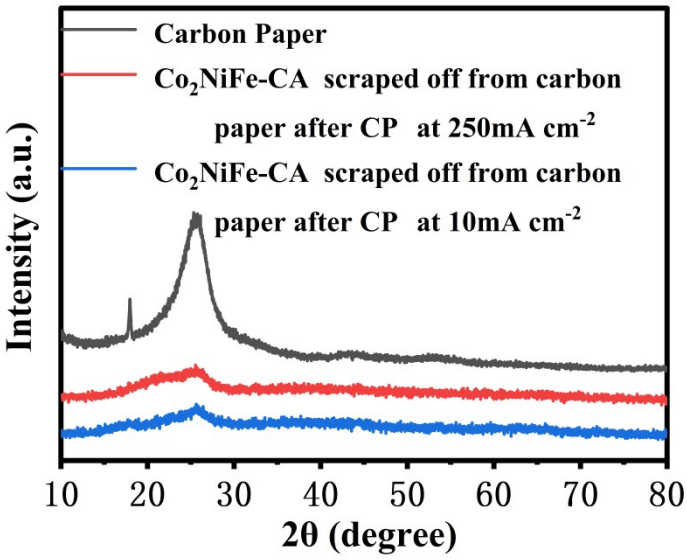


Figure S18. XRD images of carbon paper and $Co_2NiFe$-CA after CP at 10 mA $cm^{-2}$ and 250 mA $cm^{-2}$.

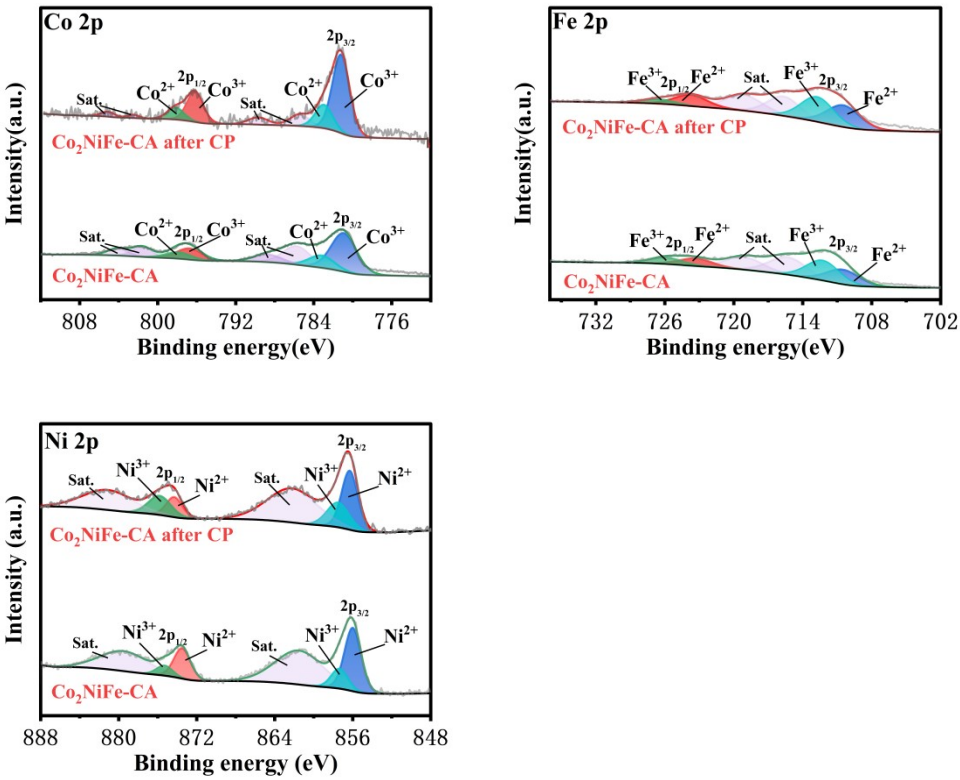


Figure S19. High resolution XPS spectra for (a) Co 2p, (b) Fe 2p and (c) Ni 2p before and after CP at 250 mA $cm^{-2}$ .

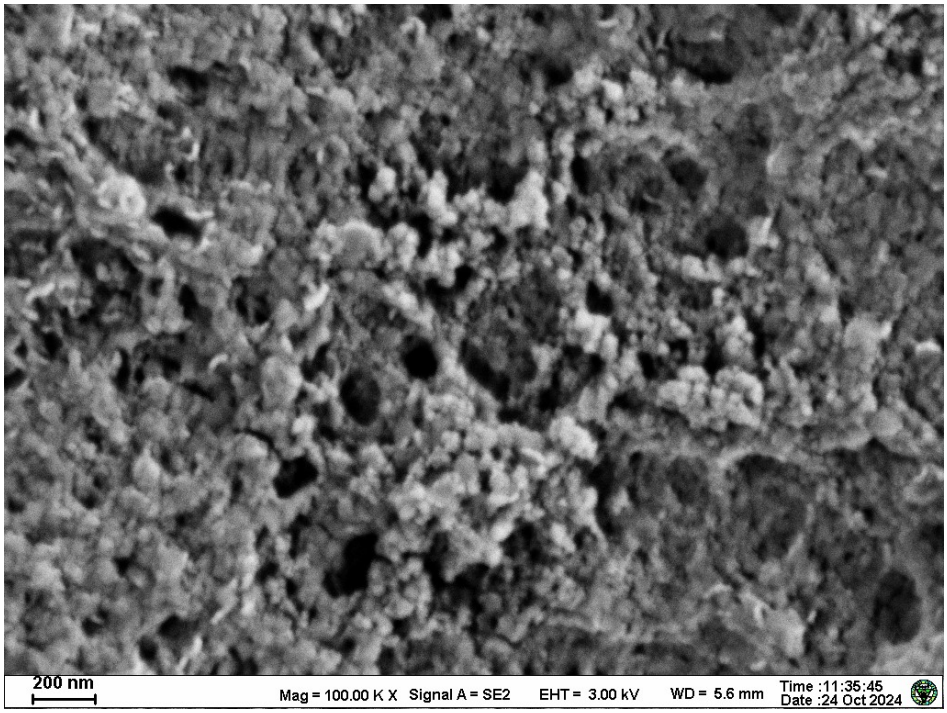

Figure S20. The SEM image of $Co_2NiFe$-CA after CP at 250 mA $cm^{-2}$ .